Journal of Quality Engineering and Production Optimization

Volume 10, Issue 1, Winter & Spring 2025

http://jqepo.shahed.ac.ir

Research Paper

DOI: 10.22070/jqepo.2026.20792.1307

Enhanced Adaptive Thresholding LASSO Control Chart Using Resubmission Method for Detecting Covariance Matrix Deviations in High-Dimensional Processes

Anahita Fathian [1], Mohammad Reza Maleki [2*], Hossein Eghbali [1]

[1] *Department of Industrial Engineering, University of Eyvanekey, Semnan, Iran*

[2] *Industrial Engineering Group, Golpayegan College of Engineering, Isfahan University of Technology, Golpayegan, Iran*

**** Corresponding Author:** Mohammad Reza Maleki (Email: m.maleki@iut.ac.ir)*

Abstract –With the increasing complexity of modern manufacturing systems and the growing dimensionality of quality data, the need for effective tools to track covariance matrix shifts in high-dimensional processes has become more urgent. This study proposes an enhanced adaptive thresholding LASSO-based control chart that utilizes a resubmission technique to enable faster detection of covariance matrix shifts in such processes. The performance of the proposed chart is compared to the classical adaptive thresholding LASSO control chart through Monte Carlo simulations. To this end, seven out-of-control scenarios are defined for the covariance matrix, including two diagonal cases, two purely off-diagonal cases, and three mixed diagonal/off-diagonal cases. The detection power of both the proposed and existing control charts is evaluated using three key metrics: average run length (ARL), standard deviation of run length (SDRL), and median run length (MRL). Simulation results indicate that the proposed resubmission-based adaptive thresholding LASSO control chart outperforms its classical counterpart in detecting disturbances in the covariance matrix. This improvement is particularly evident when simultaneous changes occur in both diagonal and off-diagonal elements. Finally, the practical application of the proposed control chart is illustrated through a case study from the automotive component industry in Iran.

***Keywords**– High-dimensional Data, Resubmission Method, Adaptive Thresholding LASSO, Covariance Matrix, Phase II.*

I. INTRODUCTION

Researchers and practitioners in statistical quality control have consistently aimed to design control charts that effectively identify and signal out-of-control conditions when a process deviates from its stable state. Recognizing the importance of sampling strategies in the performance of statistical control charts, quality engineering researchers have started integrating these techniques into various control chart types. Among these efforts are the integration of control charts with repetitive sampling (Saleh et al., 2024), ranked set sampling (Nawaz and Han, 2020), resubmission method (Arshad et al., 2024), and multiple dependent state sampling (Zhou et al., 2017). Below, recent attempts to incorporate

Manuscript Received:19-Nov-2024 & Revised:1-Feb-2025 & Accepted: 5-Apr-2025
ISSN: 2423-3781

structured sampling techniques into control chart design are outlined.

The double exponentially weighted moving average (DEWMA) control chart equipped with repetitive sampling was introduced by Adeoti (2018) to improve the early detection of small shifts in the mean parameter of normally distributed variables. The results showed that the proposed chart is more effective than the conventional DEWMA chart in identifying small changes. Noor-ul-Amin et al. (2021) developed three improved control charts for monitoring process mean based on sampling designs: paired double ranked set sampling (PDRSS), extreme paired double ranked set sampling (EPDRSS), and quartile paired double ranked set sampling (QPDRSS). Using both simulated and real-world data, they demonstrated that the control chart based on the QPDRSS method has a superior ability to detect mean shifts compared to the other designs. To improve the rapid detection of small to moderate shifts in the process location parameter, Hyder et al. (2022) equipped exponentially weighted moving average (EWMA) and cumulative sum (CUSUM) control charts with a modified successive sampling approach. They validated the practical applicability of the proposed charts using real-world data on aquatic toxicity.

Rao et al. (2024) employed a generalized multiple dependent state (GMDS) sampling approach to accelerate the detection of shifts in the coefficient of variation (CV). They assessed the performance of their proposed control chart by comparing it to similar schemes based on simple random sampling (SRS) and conventional multiple dependent state (MDS) sampling. To accelerate the detection of process dispersion anomalies, Mahmood et al. (2025) developed enhanced EWMA and CUSUM control charts using a modified successive sampling method. For further information on improved control charts using structured sampling techniques, see the studies by Arshad et al. (2021), Haq (2024), Riaz et al. (2025), and Hajiesmaeili et al. (2025).

One effective approach to enhancing the sensitivity of control charts is the resubmission method, first introduced by Govindaraju and Ganesalingam (1997) in acceptance sampling. Arshad et al. (2024) integrated the resubmission method into the design of variable control charts for the first time, specifically focusing on the $\overline{X}$ chart as a special case. The resubmission method entails that, in cases of uncertainty, the results of a sample drawn from a lot may be disregarded due to contractual stipulations. A new sample is then drawn from the same lot, without any changes to the previously selected units, and used to determine whether to accept or reject the lot. This sampling scheme allows for a variable number of rounds to reach a final decision based on satisfaction criteria. Consequently, the resubmission method provides significant support in addressing uncertainties regarding lot quality.

On the other hand, recent advancements in data acquisition technologies, such as sensors, along with the emergence of computational tools and software, have enabled the monitoring of various product features in industrial and service applications, including semiconductor manufacturing and automotive assembly. Under such conditions, quality control engineers and specialists are required to monitor high-dimensional data, which involves repeatedly measuring large volumes of observations. To effectively tackle the complex challenges of these data structures, conventional multivariate statistical process control charts require methodological enhancements. In particular, multivariate statistical process control (MSPC) charts are typically designed based on the assumption that the sample size exceeds the number of quality characteristics. However, in many industrial and service applications, financial constraints and time limitations often prevent the collection of samples as large as the problem dimension. Consequently, conventional MSPC charts face fundamental challenges under these conditions. These challenges become more critical when the shift magnitude in the distribution parameters of quality characteristics is small. Another critical issue in monitoring high-dimensional processes is the singularity of the sample covariance matrix, which leads to a determinant of zero. As a result, the inverse of the sample covariance matrix, the precision matrix, cannot be calculated. A further important issue in high-dimensional processes is that the probability of all variables or process parameters simultaneously deviating from their nominal values is extremely small. A key challenge here is that assignable causes affect only a limited number of components in the mean vector and covariance matrix, a phenomenon commonly known as a sparse shift. Under these conditions, MSPC charts lack sufficient capability to detect sparse shifts in the distribution parameters of quality characteristics. Fortunately, recent attention has been drawn to advanced approaches for monitoring process parameters in high-dimensional settings, which are discussed below.

Abdella et al. (2017) introduced a multivariate CUSUM chart using a variable selection approach to improve the detection of mean vector shifts in Phase II monitoring of high-dimensional processes. They demonstrated that when product quality involves numerous quality characteristics, incorporating variable selection into the multivariate CUSUM chart significantly increases its sensitivity to detecting process disturbances. Ahmad and Ahmed (2021) examined the asymptotic distribution of the T^2 statistic for monitoring multivariate processes when the process dimension exceeds the sample size. Their proposed monitoring approach presents several advantages: (1) it is conceptually straightforward, (2) it requires no restrictive assumptions, (3) it establishes a unified control limit framework for both Phase I and Phase II, and (4) it is applicable to both individual observations and subgroup data. Kim and Turkoz (2022) proposed a Phase II monitoring approach using a Bayesian framework for high-dimensional processes, accounting for the stochastic behavior of the process. A key feature of their proposed control chart is the adaptive selection of suspicious variables based on information from previously collected samples.

Variable selection-based control charts typically assume that only in-control data are available for the establishment of control limits. However, modern industrial processes often include out-of-control observations in reference samples. To address this issue, Zhang et al. (2023) introduced a sensitized control chart that combines a variable selection approach with a classification algorithm for monitoring high-dimensional processes. Bodnar et al. (2024) investigated how target process misspecification during Phase I analysis affects the performance of various multivariate exponentially weighted moving average (MEWMA) control charts in high-dimensional settings. They found that control charts based on Euclidean distance and diagonalized Euclidean distance are robust to fitting errors in moderate dimensions; however, in high-dimensional settings, they tend to overestimate in-control *ARL*s. To detect both sparse and non-sparse shifts in the covariance matrix of high-dimensional processes, Saemian et al. (2025) used MDS and GMDS sampling designs to design a ridge penalized likelihood ratio (RPLR) monitoring scheme. Their findings in terms of *ARL* and *SDRL* metrics indicated that the proposed charts outperform the existing RPLR chart across three types of shifts: diagonal, non-diagonal, and mixed. The development of statistical techniques for monitoring high-dimensional processes has also been explored by other researchers, such as Feng et al. (2020), Ye and Liu (2022), Huang et al. (2023), Jafari et al. (2023), Sun et al. (2024), and Oyegoke et al. (2025). Additionally, Jalilibal et al. (2024) have provided a systematic classification of online monitoring techniques for high-dimensional processes.

As previously noted, to accelerate the detection of small to moderate shifts in the process mean, Arshad et al. (2024) enhanced the $\overline{X}$ control chart using a resubmission-based sampling scheme. To the best of the authors' knowledge, no other study has addressed the design of control charts incorporating the resubmission method. Given that in modern applications of statistical quality control, product quality is expressed through numerous quality characteristics, this paper introduces an improved version of the adaptive thresholding LASSO control chart that incorporates a resubmission approach to capture covariance disturbances in high-dimensional settings.

This article is organized as follows: Section 2 introduces the adaptive thresholding LASSO statistic used for Phase II monitoring of high-dimensional processes. The improved version of the adaptive thresholding LASSO control chart based on the resubmission method is presented in Section 3. In Section 4, the performance of the proposed control chart is compared to the classical version of the adaptive thresholding LASSO chart through Monte Carlo simulations. The practical applicability of the proposed chart is validated through a case study in the automotive parts industry in Section 5. Finally, Section 6 presents the conclusions and provides recommendations for future research.

II. ADAPTIVE THRESHOLDING LASSO CHART

This section first introduces the classical Lasso-based adaptive thresholding control chart. An enhanced version of this chart is then designed using the resubmission approach. To ensure consistent notation and clarify the concepts, all abbreviations are summarized in Table I.

Table I. Notations

Notation	Description
Indices	
i	Sample index
j	Observation index
k , l	Variable index
Distribution parameters	
Y_k	The k^{th} variable
$\boldsymbol{\mu}_{IC}$	In-control mean vector
$\boldsymbol{\Sigma}_{IC}$	In-control covariance matrix
$\boldsymbol{\Sigma}_{OC}$	Out-of-control covariance matrix
μ_k	Nominal mean of the k^{th} variable
σ_k^2	Nominal variance of the k^{th} variable
θ_{kl}	Variance of random variable $\hat{d}_{i,kl}$
γ_{kl}^*	Threshold value of $d_{i,kl}$
Sample parameters	
$\mathbf{Y}_i$	Matrix of observations at the i^{th} sampling point
$\mathbf{y}_{ij}$	Column vector of the j^{th} observation at the i^{th} sample
y_{ijk}	The j^{th} observation of the k^{th} variable in the i^{th} sample
$\overline{\mathbf{y}}_i$	Sample mean vector at the i^{th} sample
$\overline{y}_{ik}$	Sample mean of the k^{th} variable at the i^{th} sample
$\mathbf{S}_i$	Sample covariance matrix for the i^{th} sample
$S_{i,k}^2$	Sample variance of the k^{th} variable at the i^{th} sample
$S_{i,lk}$	Covariance between variables k and l
$\mathbf{D}_i$	Difference matrix at the i^{th} sample
$d_{i,kl}$	The component in the k^{th} row and l^{th} column of matrix $\mathbf{D}_i$
$\hat{\mathbf{D}}_i$	Shrunken difference matrix
$\hat{d}_{i,kl}$	The component in the k^{th} row and l^{th} column of matrix $\hat{\mathbf{D}}_i$
$A-COV_i$	Adaptive thresholding lasso statistic for the i^{th} sample

Continue Table I. Notations

Notation	Description
Chart parameters	
n	Number of observations within each sample
p	Number of variables under investigation
φ	Regularization parameter
η	Shrinkage parameter
m	Resubmission scheme parameter
UCL_{A-COV}	Upper control limit of classical adaptive thresholding LASSO chart
UCL'_{A-COV}	Upper control limit of resubmission-based adaptive thresholding LASSO chart
Other parameters	
τ	Change point
T	Signal point
$\mathbf{I}_p$	p - dimensional identity matrix
α	Probability of type I error
ARL_{IC}	In-control average run length

Consider a process where product quality is characterized by p quality characteristics, $Y_1, Y_2, ..., Y_p$ each of which follows a normal distribution. The observation matrix at the i^{th} sampling point is represented by a $p \times n$ dimensional matrix $\mathbf{Y}_i = \left(\mathbf{y}_{i1}, \mathbf{y}_{i2}, ..., \mathbf{y}_{in}\right)$, where $\mathbf{y}_{ij} = \left(y_{ij1}, y_{ij2}, ..., y_{ijp}\right)^T$ is a *p*-dimensional column vector representing the values of the quality characteristics for the j^{th} observation in the i^{th} sample. Furthermore, $y_{ijk}; j = 1, 2, ..., n; k = 1, 2, ..., p$ denotes the value of the k^{th} quality characteristic in the j^{th} observation of the i^{th} sample. In this paper, it is assumed that the process mean vector and covariance matrix denoted by $\boldsymbol{\mu}_{IC} = \left(\mu_1, \mu_2, ..., \mu_p\right)^T$ and $\boldsymbol{\Sigma}_{IC} = \begin{pmatrix} \sigma_1^2 & \sigma_{12} & \cdots & \sigma_{1p} \\ \sigma_{21} & \sigma_2^2 & \cdots & \sigma_{2p} \\ \vdots & \vdots & \ddots & \vdots \\ \sigma_{p1} & \sigma_{p2} & \cdots & \sigma_p^2 \end{pmatrix}$, respectively are known based on Phase I analysis.

The sample mean vector for the i^{th} subgroup is denoted by $\bar{\mathbf{y}}_i = \left(\bar{y}_{i1}, \bar{y}_{i2}, ..., \bar{y}_{ip}\right)^T$, where $\bar{y}_{ik} = \frac{1}{n}\sum_{j=1}^{n} y_{ijk}$. Moreover, the diagonal and off-diagonal elements of the sample covariance matrix in the i^{th} subgroup are calculated according to Equations (1) and (2), respectively.

$$S_{i,k}^2 = \frac{1}{n-1}\sum_{j=1}^{n}\left(y_{ijk} - \bar{y}_{ik}\right)^2 \tag{1}$$

$$S_{i,lk} = \frac{1}{n-1}\sum_{j=1}^{n}\left(y_{ijk} - \overline{y}_{ik}\right)\left(y_{ijl} - \overline{y}_{il}\right) \tag{2}$$

This paper assumes that an assignable cause affects only the covariance matrix, leaving the process mean vector unchanged. In other words, upon the occurrence of the assignable cause at time τ, observation vectors for samples $i = 1,2,...,\tau$ follow a multivariate normal distribution with parameters $\mathbf{y}_{ij} \sim MVN\left(\boldsymbol{\mu}_{IC}, \boldsymbol{\Sigma}_{IC}\right)$, while observation vectors for samples $i = \tau+1, \tau+2,...,T$ follow a multivariate normal as $\mathbf{y}_{ij} \sim MVN\left(\boldsymbol{\mu}_{IC}, \boldsymbol{\Sigma}_{OC}\right)$, such that $\boldsymbol{\Sigma}_{OC} \neq \boldsymbol{\Sigma}_{IC}$. Accordingly, this paper aims to quickly detect shifts in the covariance matrix as early as possible by testing the null hypothesis $H_0 : \boldsymbol{\Sigma} = \boldsymbol{\Sigma}_{IC}$ against the alternative hypothesis $H_1 : \boldsymbol{\Sigma} \neq \boldsymbol{\Sigma}_{IC}$. To conduct this hypothesis test using the adaptive thresholding LASSO technique, the target and sample covariance matrices are subtracted to form a difference matrix for the i^{th} sample as follows:

$$\mathbf{D}_i = \mathbf{S}_i - \boldsymbol{\Sigma}_{IC} = \begin{pmatrix} d_{i,11} & d_{i,12} & \dots & d_{i,1p} \\ d_{i,21} & d_{i,22} & \dots & d_{i,2p} \\ \vdots & \vdots & \ddots & \vdots \\ d_{i,p1} & d_{i,p2} & \dots & d_{i,pp} \end{pmatrix} \tag{3}$$

In high-dimensional settings, an assignable cause typically affects only a small subset of the elements in the covariance matrix. Consequently, even when the process dispersion is statistically out-of-control, many elements of the difference matrix remain close to zero. It is important to note that when the dispersion matrix is in-control, the elements of the difference matrix $\mathbf{D}_i$ are not exactly zero. Thus, to convert the difference matrix into a sparse matrix with predominantly zero elements, each element is shrunk using the following formula:

$$\hat{d}_{i,kl} = d_{i,kl}\left(1 - \left|\frac{\gamma^*_{kl}}{d_{i,kl}}\right|^{\eta}\right)_+ \tag{4}$$

In Equation (4), η is the shrinkage parameter, and γ^*_{kl} denotes the threshold value for the element $d_{i,kl}$, computed as:

$$\gamma^*_{kl} = \varphi\left(\frac{\theta_{kl}}{n}\log p\right)^{0.5} \tag{5}$$

In equation (5), φ represents the regularization parameter. To compute $\left(1 - \left|\gamma^*_{kl} \big/ d_{i,kl}\right|^{\eta}\right)_+$ in Equation (4), the value of $\left|\gamma^*_{kl} \big/ d_{i,kl}\right|^{\eta}$ is considered. If $\left|\gamma^*_{kl} \big/ d_{i,kl}\right|^{\eta} < 1$, then $\left(1 - \left|\gamma^*_{kl} \big/ d_{i,kl}\right|^{\eta}\right)_+ = 1 - \left|\gamma^*_{kl} \big/ d_{i,kl}\right|^{\eta}$; otherwise, if $\left|\gamma^*_{kl} \big/ d_{i,kl}\right|^{\eta} \geq 1$, then $\left(1 - \left|\gamma^*_{kl} \big/ d_{i,kl}\right|^{\eta}\right)_+ = 0$. Furthermore, θ_{kl} denotes the variance of the random variable $\hat{d}_{i,kl}$,

calculated using the following equation:

$$\theta_{kl} = \sigma_k^2 \sigma_l^2 + \left(\sigma_{kl}\right)^2 \tag{6}$$

The value of the adaptive thresholding LASSO statistic for monitoring the sample covariance matrix at the i^{th} subgroup is calculated according to the following formula:

$$A - COV_i = \sum_{k=1}^{p} \sum_{l=1}^{p} \left(\frac{\hat{d}_{i,kl}^2}{\sigma_k^2 \sigma_l^2 + \sigma_{kl}^2} \right) \tag{7}$$

When the chart statistic exceeds the control limit, $A - COV_i > UCL_{A-COV}$, the adaptive thresholding LASSO chart triggers an out-of-control signal at the i^{th} subgroup. Since the adaptive thresholding LASSO statistic does not follow a known distribution, the upper control limit is determined through simulation to ensure that the in-control *ARL* equals a specified value of $ARL_{IC} = 1/\alpha$. It is important to note that α represents the Type I error probability, which is typically set at 0.005 or 0.0027.

III. PROPOSED RESUBMISSION-BASED CHART

As mentioned, the concept of resubmission was first introduced by Govindaraju and Ganesalingam (1997). In this plan, lot reinspection is permitted when initial inspection results are suspicious or when the supplier is authorized to conduct resampling according to the contract terms and relevant provisions. To implement the resubmission scheme, the following conditions must be met:

- The initial inspection results that led to the rejection of the sampled items must be disregarded.
- The consumer must trust the producer, and the producer must not intentionally exploit the resampling opportunity.

The operational procedure of the resubmission plan in acceptance sampling is as follows:

1. Perform the initial inspection and implement a reference sampling plan (for example a single sampling scheme with sample size n and acceptance number AC).
2. In case of rejection during the initial inspection, apply the reference plan *m* times, and reject the lot if resubmission occurs $m-1$ times.

Assume that a single sampling plan is used as the reference scheme, where $Pa(p)$ represents the probability of final acceptance of a lot with quality level p. In this scheme, resubmission is permitted up to $m-1$ times, and resampling is possible after each rejected attempt. In other words, a lot with fixed quality may be inspected up to *m* times. Therefore, the final acceptance probability of the lot under this sampling scheme is:

$$Pa(p) = P_a + (1-P_a)P_a + (1-P_a)^2 P_a + \ldots + (1-P_a)^{m-1} P_a = 1-(1-P_a)^m \tag{8}$$

Equation (8) is valid when the lot size is sufficiently large and the quality level remains constant throughout the resampling process. This equation is applicable across different reference sampling designs, including double sampling schemes. The average sample number (ASN) for the resubmission framework is calculated as follows:

$$ASN(p) = n + n(1-P_a) + n(1-P_a)^2 + ... + n(1-P_a)^{m-1} = \frac{n\left(1-(1-P_a)^m\right)}{P_a} \tag{9}$$

The idea of using a resubmission scheme designed for acceptance sampling in statistical quality control was introduced by Arshad et al. (2024). They developed a $\bar{X}$ control chart using a resubmitted sampling scheme that allows for retaking a sample for inspection at any stage if there is any doubt. It is important to note that the resubmission scheme differs from repetitive sampling, despite some similarities. In repetitive sampling, the control region is divided into three zones: acceptance, rejection, and warning. In contrast, the resubmission scheme consists of only two zones: acceptance and rejection. Building on this foundation, our study adapts the resubmission concept for high-dimensional covariance monitoring. The operational steps of the proposed resubmission-based adaptive thresholding LASSO chart, aimed at accelerating the detection of disturbances in the covariance matrix of high-dimensional processes, are outlined below:

1. Draw a random sample of size *n* from the process and calculate the sample covariance matrix, denoted as $\mathbf{S}_i$.
2. Based on Step 1, compute the difference matrix $\mathbf{D}_i$ and the shrunk difference matrix $\hat{\mathbf{D}}_i$ using equations (3) and (4), respectively.
3. Calculate the adaptive thresholding LASSO statistic for the i^{th} sample using Equation (7).
4. If $A-COV_i < UCL'_{A-COV}$, declare the process dispersion to be in-control. Otherwise, if $A-COV_i \geq UCL'_{A-COV}$, obtain another sample in resubmission and return to Step 1. It is worth noting that UCL'_{A-COV} denotes the upper control limit of the adaptive thresholding LASSO control chart equipped with the resubmission technique.
5. If the process is not declared in-control at Step 4, place the corresponding sample in a suspended state and repeat Steps 1-4 a maximum of *m* times. If the process remains suspended for all $m-1$ resubmissions, it is considered out-of-control. This means the maximum number of resubmissions is $m-1$. Fig. (2) provides a graphical representation to facilitate understanding of the proposed statistical technique.

IV. NUMERICAL EXAMPLE

The aim of this section is to assess the performance of the proposed resubmission-based adaptive thresholding LASSO control chart and compare its results with those of the classical version in terms of *ARL*, *SDRL*, and *MRL* using Monte Carlo simulation. In addition, the computational time (*CT*) in seconds required for 10,000 simulation replications in each out-of-control scenario is reported to demonstrate the efficiency of the proposed method. Note that, all simulations are performed using MATLAB R2025a on a personal computer with an Intel Core i9 processor and 16 GB of RAM. Consider a process where product quality is described using $p=15$ normally distributed quality characteristics with mean vector $\boldsymbol{\mu}_{IC} = \mathbf{0}_{15\times1}$ and covariance matrix $\boldsymbol{\Sigma}_{IC} = \mathbf{I}_P$. For both the resubmission-based and classical versions of the adaptive thresholding LASSO control charts, the sample size, regularization parameter, and shrinkage parameter are set to $n=12$, $\varphi=1$, and $\eta=4$, respectively. Note that Abdella et al. (2019) conducted extensive simulation studies across different ranges of parameters φ and η, considering small, moderate, and large values. They examined how the sensitivity of the adaptive thresholding LASSO chart varied when the shrinkage parameter ranges from 2 to 10 and the regularization parameters ranges from 0.5 to 2. They showed that the chart with smaller values of φ and larger values of η performs better in detecting small changes in the covariance matrix. Based on simulation studies under various out-of-control conditions, they selected $\eta=4$ and $\varphi=1$ to achieve balanced performance of the adaptive thresholding LASSO chart across different shift sizes.

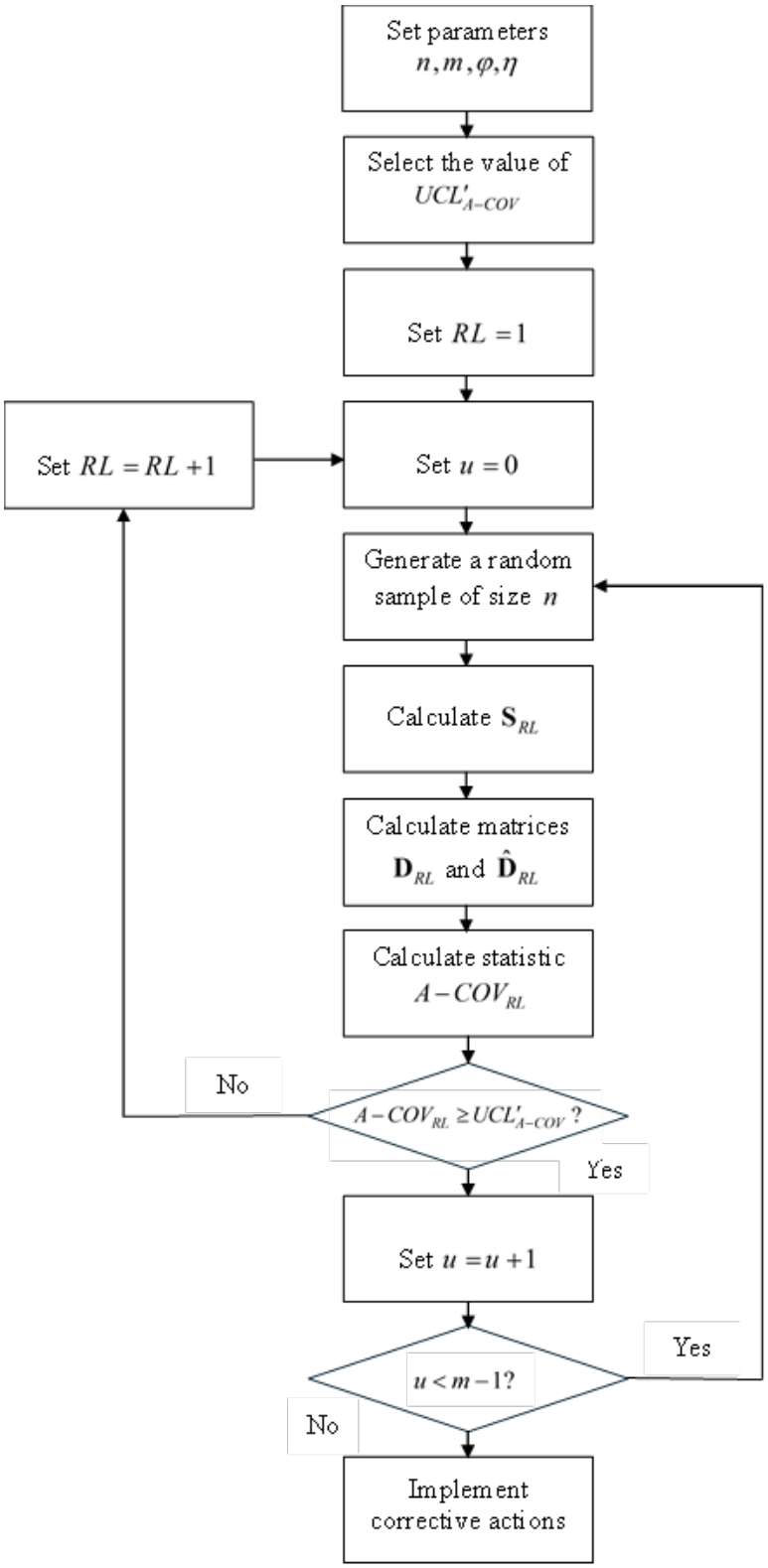

Fig. 2. Flowchart of the proposed resubmission-based monitoring scheme

Furthermore, in the proposed resubmission-based adaptive thresholding LASSO monitoring scheme, the value of m is set to 2. To ensure a fair comparison between the performance of the competing control charts, their upper control limits are calibrated based on 10,000 Monte Carlo replications to attain an in-control average run length of $ARL_{IC} = 200$ for both charts, corresponding to a Type I error probability of $\alpha = 0.005$. To achieve this, the UCL_{A-COV} value for the classical and proposed adaptive thresholding LASSO control charts are set at 0.2783 and 0.2013, respectively. Besides, the shift magnitudes for the off-target components of the process covariance matrix are set to $\delta \in \{0.05, 0.1, 0.15, 0.2, 0.25\}$. To thoroughly evaluate the competing control charts under different process conditions, seven out-of-control scenarios are considered, along with the specified shift magnitudes. These scenarios are intentionally designed to assess chart performance across a variety of realistic disturbance patterns, as discussed below.

Diagonal pattern: These scenarios involve diagonal shifts, where changes occur solely in the variance components along the main diagonal of the process covariance matrix. We examine two diagonal scenarios corresponding to Equations (10) and (11). In the first scenario, all variance elements are changed simultaneously. In the second scenario, only the variance of the first quality characteristic is changed from 1 to $1+\delta$.

$$\boldsymbol{\Sigma}_{1,out} = \boldsymbol{\Sigma}_0 + \boldsymbol{\Delta}_{1,out}; \boldsymbol{\Delta}_{1,out} = \begin{pmatrix} \delta & 0 & \dots & 0 \\ 0 & \delta & \dots & 0 \\ \vdots & \vdots & \ddots & \vdots \\ 0 & 0 & \dots & \delta \end{pmatrix}_{15\times 15} \tag{10}$$

$$\boldsymbol{\Sigma}_{2,out} = \boldsymbol{\Sigma}_0 + \boldsymbol{\Delta}_{2,out}; \boldsymbol{\Delta}_{2,out} = \begin{pmatrix} \delta & 0 & \dots & 0 \\ 0 & 0 & \dots & 0 \\ \vdots & \vdots & \ddots & \vdots \\ 0 & 0 & \dots & 0 \end{pmatrix} \tag{11}$$

Off-diagonal pattern: These scenarios reflect changes in the off-diagonal elements of the process covariance matrix, which indicate disturbances in the covariance components that simulate structural dependencies among quality characteristics. Two off-diagonal scenarios, corresponding to Equations (12) and (13), are examined. In these settings, the covariance values for seven and three quality characteristics are increased by Δ, respectively.

$$\boldsymbol{\Sigma}_{3,out} = \boldsymbol{\Sigma}_0 + \boldsymbol{\Delta}_{3,out}; \boldsymbol{\Delta}_{3,out} = \begin{pmatrix} 0 & \delta & \dots & \delta & 0 & \dots & 0 \\ \delta & 0 & \dots & \delta & 0 & \dots & 0 \\ \vdots & \vdots & \ddots & \vdots & \vdots & \ddots & \vdots \\ \delta & \delta & \dots & 0 & 0 & \dots & 0 \\ 0 & 0 & \dots & 0 & 0 & \dots & 0 \\ \vdots & \vdots & \ddots & \vdots & \vdots & \ddots & \vdots \\ 0 & 0 & \dots & 0 & 0 & \dots & 0 \end{pmatrix} \tag{12}$$

Combined diagonal/off-diagonal pattern: These configurations involve simultaneous changes in both the variance and covariance components of the process covariance matrix. The simulations in this section examine three combined scenarios, corresponding to Equations (14) to (16).

$$\boldsymbol{\Sigma}_{4,out}=\boldsymbol{\Sigma}_0+\boldsymbol{\Delta}_{4,out};\boldsymbol{\Delta}_{4,out}=\begin{pmatrix}0&\delta&\delta&0&\dots&0\\\delta&0&\delta&0&\dots&0\\\delta&\delta&0&0&\dots&0\\0&0&0&0&\dots&0\\\vdots&\vdots&\vdots&\vdots&\ddots&\vdots\\0&0&0&0&\dots&0\end{pmatrix}_{15\times15} \tag{13}$$

$$\boldsymbol{\Sigma}_{5,out}=\boldsymbol{\Sigma}_0+\boldsymbol{\Delta}_{5,out};\boldsymbol{\Delta}_{5,out}=\begin{pmatrix}\delta&\delta&\delta&\delta&0&\dots&0\\\delta&\delta&\delta&\delta&0&\dots&0\\\delta&\delta&\delta&\delta&0&\dots&0\\\delta&\delta&\delta&\delta&0&\dots&0\\0&0&0&0&0&\dots&0\\\vdots&\vdots&\vdots&\vdots&\vdots&\ddots&\vdots\\0&0&0&0&0&\dots&0\end{pmatrix}_{15\times15} \tag{14}$$

$$\boldsymbol{\Sigma}_{6,out}=\boldsymbol{\Sigma}_0+\boldsymbol{\Delta}_{6,out};\boldsymbol{\Delta}_{6,out}=\begin{pmatrix}\delta^2&\delta&\delta&0&\dots&0\\\delta&\delta^2&\delta&0&\dots&0\\\delta&\delta&\delta^2&0&\dots&0\\0&0&0&0&\dots&0\\\vdots&\vdots&\vdots&\vdots&\ddots&\vdots\\0&0&0&0&\dots&0\end{pmatrix}_{15\times15} \tag{15}$$

$$\boldsymbol{\Sigma}_{7,out}=\boldsymbol{\Sigma}_0+\boldsymbol{\Delta}_{7,out};\boldsymbol{\Delta}_{7,out}=\begin{pmatrix}\delta&\delta&\delta&0&\dots&0&0&0&0\\\delta&\delta&\delta&0&\dots&0&0&0&0\\\delta&\delta&\delta&0&\dots&0&0&0&0\\0&0&0&0&\dots&0&0&0&0\\\vdots&\vdots&\vdots&\vdots&\ddots&\vdots&\vdots&\vdots&\vdots\\0&0&0&0&\dots&0&0&0&0\\0&0&0&0&\dots&0&\delta&\delta&\delta\\0&0&0&0&\dots&0&\delta&\delta&\delta\\0&0&0&0&\dots&0&\delta&\delta&\delta\end{pmatrix}_{15\times15} \tag{16}$$

Table II reports the resulting *ARL*s, *SDRL*s, *MRL*s, and *CT*s for the proposed and existing adaptive thresholding LASSO charts under the first diagonal scenario for $\delta\in\{0.05,0.1,0.15,0.2,0.25\}$. The table shows that the resubmission-based adaptive thresholding LASSO chart consistently achieves lower *ARL* values across all shift levels than the classical version, highlighting its improved detection sensitivity when all diagonal elements deviate from their nominal values. The reduction in the *ARL* index from incorporating the resubmission technique into the adaptive thresholding LASSO control chart for shift magnitudes of 0.05, 0.10, 0.15, 0.20, and 0.25 is 15.6530, 7.2485, 2.6595,

1.3730, and 0.6775, respectively. This shows that the proposed control chart is faster than the existing adaptive thresholding LASSO chart at these shift levels by 32.38%, 45.54%, 41.39%, 41.09%, and 31.92%, respectively. Another important point is that as the shift magnitude increases, the improvement in the *ARL* index initially increases and then decreases. The greatest relative improvement occurs at $\delta = 0.1$, while the smallest improvement is seen at $\delta = 0.25$. Specifically, the proposed control chart shows greater improvements for moderate shifts $\delta \in \{0.1, 0.15, 0.2\}$ compared to the existing chart. Additionally, the proposed resubmission-based chart has a lower *MRL* index across all shift magnitudes, except for $\delta = 0.2$. Additionally, Fig. 2 illustrates the *ARL* curves of the two charts for clarity.

Table II. Run length behavior of competing charts under the first diagonal scenario

Chart	Control limit	Index	δ					
			0	**0.05**	**0.1**	**0.15**	**0.2**	**0.25**
LASSO-RSB	0.2013	*ARL*	204.9480	32.6850	8.6645	3.7660	1.9695	1.4465
		SDRL	210.0123	31.1223	9.0263	3.2327	1.3467	0.7736
		MRL	143.5	24	6	3	2	1
		CT	458.955	26.705	9.204	4.516	2.788	2.236
LASSO-classic	0.2783	*ARL*	200.3697	48.3380	15.9130	6.4255	3.3425	2.1240
		SDRL	200.9690	48.3286	15.5828	5.9943	2.7771	1.5329
		MRL	143.5	33	11	5	2	2
		CT	81.960	22.047	7.471	3.716	2.340	1.900

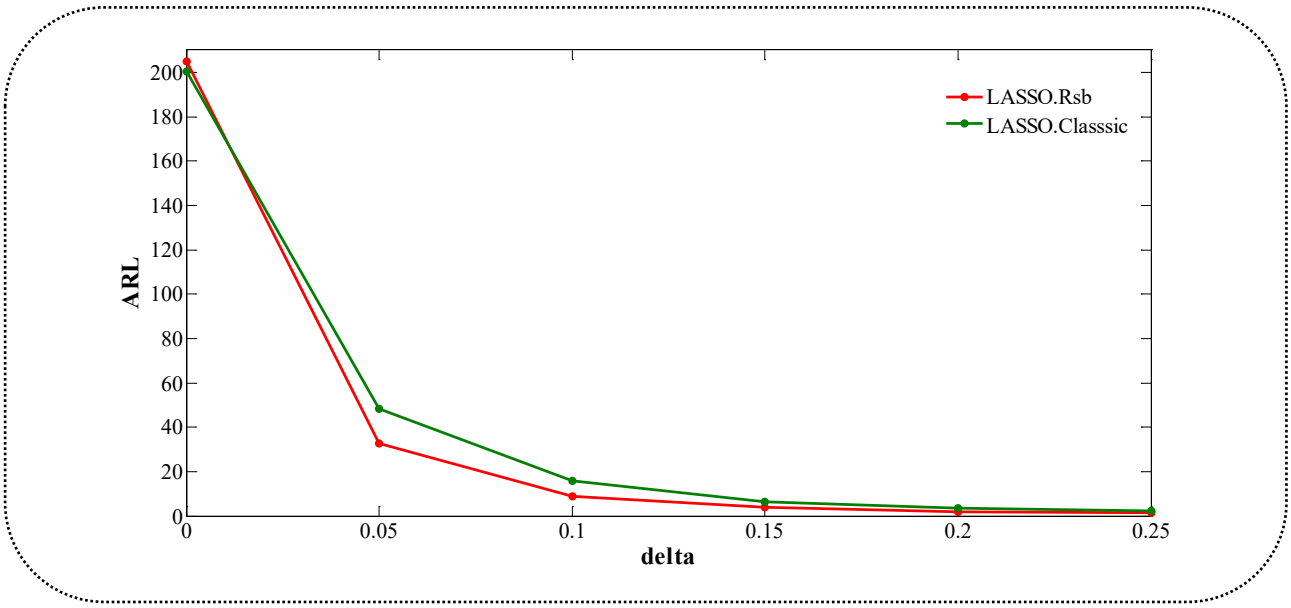

Fig. 2. *ARL* curve for the first diagonal scenario

Table III presents the *ARL*, *SDRL*, *MRL,* and *CT* values for both the proposed and conventional adaptive thresholding LASSO control charts, evaluated under the second diagonal scenario at $\delta \in \{0.05, 0.1, 0.15, 0.2, 0.25\}$. According to the results in Table III, the proposed adaptive thresholding LASSO control chart equipped with the

resubmission technique is more sensitive to the second diagonal out-of-control scenario than its classical counterpart. The incorporation of the resubmission technique reduces the ARL index for shift magnitudes of 0.05, 0.10, 0.15, 0.20, and 0.25 by 11.5995, 9.4905, 17.7685, 16.7380, and 13.0625 units, respectively. Consequently, the proposed chart demonstrates superior power, outperforming the conventional adaptive thresholding LASSO chart with enhanced detection power of 6.41%, 6.03%, 12.43%, 13.40%, and 11.81% at the corresponding shift levels. The most significant improvement in detection power from incorporating the resubmission technique in the adaptive thresholding LASSO chart occurs at a shift level of $\delta = 0.2$, while the least improvement is observed at $\delta = 0.1$. Additionally, the performance improvement from implementing the resubmission method in designing the adaptive thresholding LASSO chart is substantially greater in the first diagonal scenario than in the second. Table III shows that the proposed control chart consistently exhibits lower *MRL* values across all shift magnitudes compared to the classical adaptive thresholding LASSO chart. For shift magnitudes of 0.05, 0.10, 0.15, 0.20, and 0.25, the *MRL* values of the proposed chart are lower by 15, 9, 16, 11, and 9 units, respectively, resulting in relative improvements of 11.49%, 8.11%, 15.53%, 13.25%, and 11.54%. For illustrative clarity, Fig. 3 depicts the *ARL* curves of the classical and resubmission-based control charts.

Table III. Run length behavior of competing charts under the second diagonal scenario

Chart	Control limit	Index	δ					
			0	**0.05**	**0.1**	**0.15**	**0.2**	**0.25**
LASSO-RSB	0.2013	*ARL*	204.9480	169.4825	147.7950	125.2235	108.1625	97.5420
		SDRL	210.0123	172.5259	146.8628	124.7001	110.5642	94.2214
		MRL	143.5	115.5	102	87	72	69
		CT	458.955	157.049	114.691	100.508	85.386	72.804
LASSO-classic	0.2783	*ARL*	200.3697	181.0820	157.2855	142.9920	124.9005	110.6045
		SDRL	200.9690	176.6170	152.9787	139.9755	128.4393	106.4787
		MRL	143.5	130.5	111	103	83	78
		CT	81.960	75.005	62.670	57.318	47.452	44.112

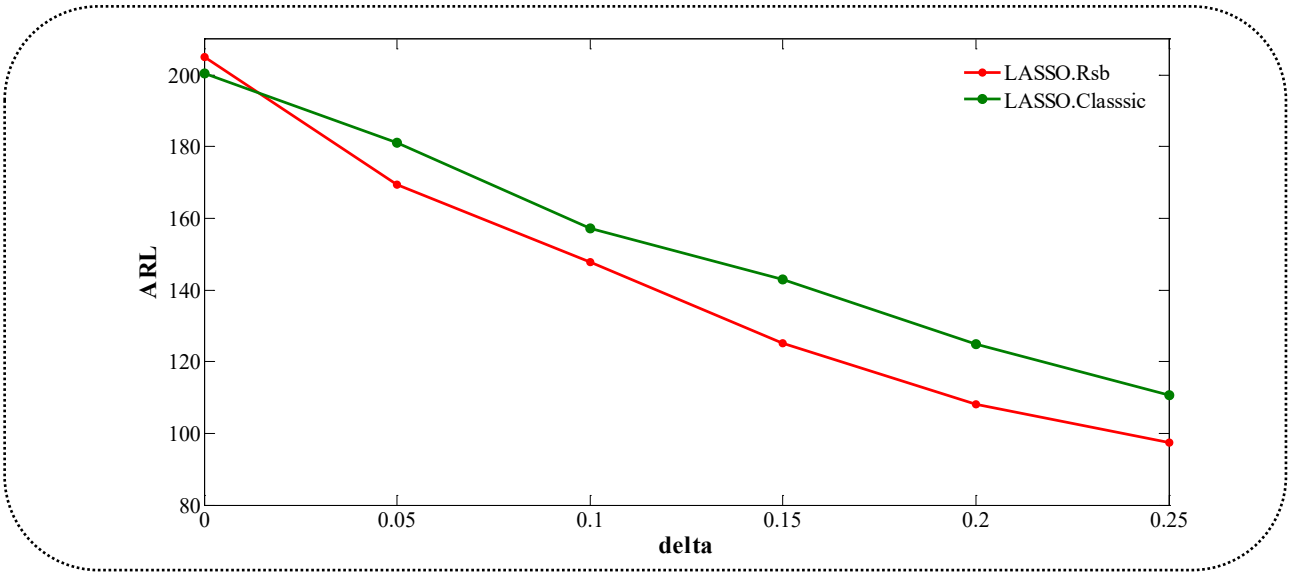

Fig. 3. *ARL* curve for the second diagonal scenario

The extracted *ARL*, *SDRL*, *MRL* and *CT* values for both the proposed and existing adaptive thresholding LASSO charts under the first off-diagonal pattern across shift magnitudes of $\delta \in \{0.05, 0.1, 0.15, 0.2, 0.25\}$ are presented in Table IV. The results summarized in Table 4 and Fig. 4 indicate that the classical and resubmission-based versions of the adaptive thresholding LASSO chart produce approximately similar *ARL* values. Although the two methods yield relatively similar results for the *ARL* index, the proposed adaptive thresholding LASSO control chart shows a lower *SDRL* than its classical counterpart. This improvement ranges from a minimum of 13.07% to a maximum of 22.86% across all levels of δ .

Table IV. Run length behavior of competing charts under the first off-diagonal scenario

Chart	Control limit	Index	δ					
			0	**0.05**	**0.1**	**0.15**	**0.2**	**0.25**
LASSO-RSB	0.2013	*ARL*	204.9480	139.0540	59.9060	21.1355	8.8015	4.3215
		SDRL	210.0123	131.2982	59.9970	20.1514	8.2364	3.8413
		MRL	143.5	99	43	7	6	3
		CT	458.955	116.975	46.080	16.912	8.144	4.988
LASSO-classic	0.2783	*ARL*	200.3697	139.4150	56.5005	20.0905	8.5980	4.5715
		SDRL	200.9690	140.4884	55.3184	19.2454	8.2728	4.1211
		MRL	143.5	95	41	14	6	3
		CT	81.960	58.911	24.706	8.793	4.785	2.906

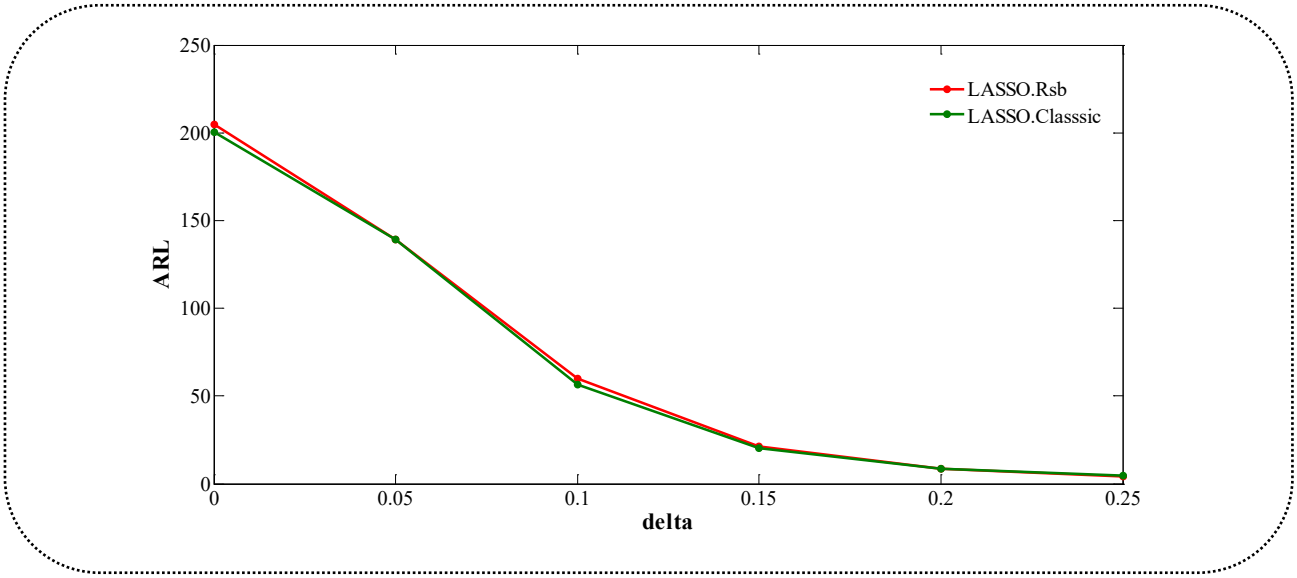

Fig. 4. *ARL* curve for the first off-diagonal scenario

Table V presents the run length properties as well as *CT* values for both the proposed and existing adaptive thresholding LASSO charts under the second off-diagonal pattern across various shift magnitudes. Besides, Fig. 5 presents a graphical comparison of the *ARL* curves for the competing control charts. The results indicate that, except for $\delta = 0.05$, the proposed resubmission-based control chart is more effective in detecting out-of-control Pattern II. Specifically, equipping the adaptive thresholding LASSO chart with the resubmission procedure yields improvements

in *ARL* of 4.29%, 2.37%, 4.90%, and 8.57% for shift magnitudes of 0.10, 0.15, 0.20, and 0.25, respectively. As the shift magnitude in the off-diagonal elements of the covariance matrix increases, the advantage of the proposed chart over the classical adaptive thresholding LASSO chart becomes increasingly evident. Overall, the analysis of Tables II - V indicates that the superiority of the proposed adaptive thresholding LASSO control chart over the existing version is more evident in scenarios where the assignable cause affects the diagonal elements of the covariance matrix rather than the off-diagonal elements.

Table V. Run length behavior of competing charts under the second off-diagonal scenario

Chart	Control limit	Index	δ					
			0	**0.05**	**0.1**	**0.15**	**0.2**	**0.25**
LASSO-RSB	0.2013	*ARL*	204.9480	187.7260	159.2255	133.7775	94.7285	63.2485
		SDRL	210.0123	184.1668	158.9501	128.0736	96.9427	65.4011
		MRL	143.5	138	112	96	64	42.5
		CT	458.955	158.219	144.224	99.389	73.594	68.975
LASSO-classic	0.2783	*ARL*	200.3697	185.0230	166.3810	137.0325	99.6065	69.1715
		SDRL	200.9690	186.6191	161.2937	141.4794	95.3958	67.0353
		MRL	143.5	127	118.5	93	71.5	51
		CT	81.960	78.396	62.974	50.478	41.702	26.818

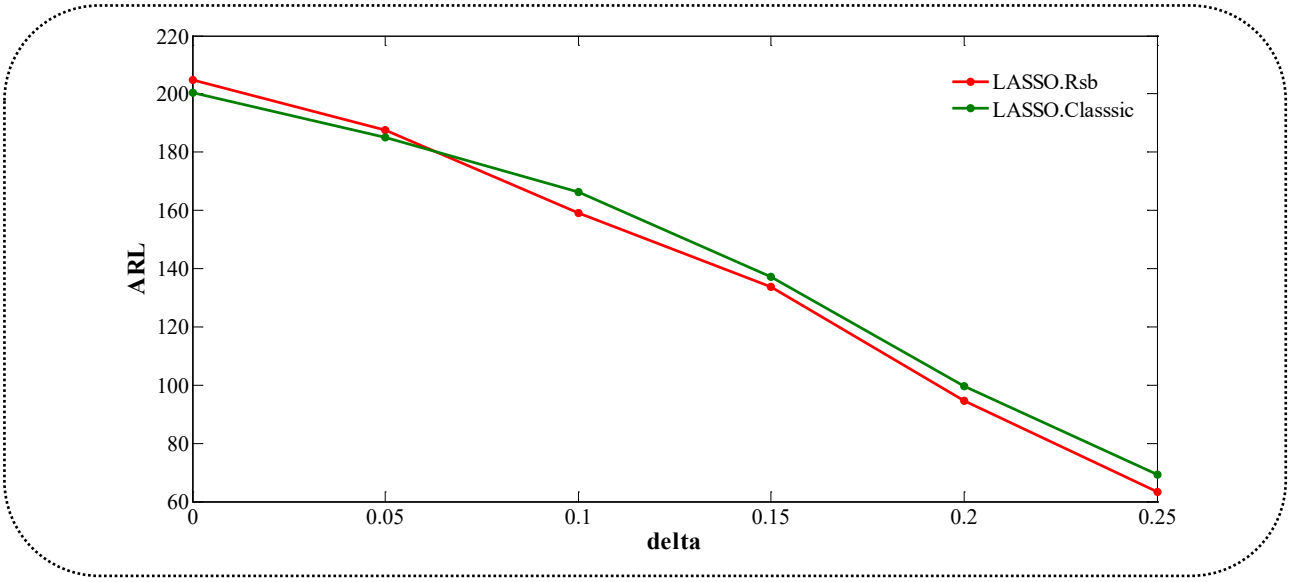

Fig. 5. *ARL* curve for the second off-diagonal scenario

The run length characteristics and *CT* values of both the proposed resubmission-based and classical adaptive thresholding LASSO charts under the first combined diagonal/off-diagonal shift pattern for shift levels $\delta \in \{0.05, 0.1, 0.15, 0.2, 0.25\}$ are reported in Table VI and Fig. 6. The results indicate that, for all δ values, the proposed chart achieves smaller *ARL*s than the classical adaptive thresholding LASSO chart, demonstrating its superior sensitivity to the first combined diagonal/off-diagonal pattern. The *ARL* improvements for shift magnitudes of 0.05, 0.10, 0.15, 0.20, and 0.25 are 16.01, 14.12, 8.97, 3.86, and 2.23 units, respectively. This confirms that incorporating the

resubmission method into the adaptive thresholding LASSO control chart results in *ARL* improvements of 12.85%, 22.42%, 28.73%, 24.78%, and 25.38% for the respective δ levels. The maximum *ARL* improvement occurs at $\delta = 0.15$ (28.73%), while the minimum is at $\delta = 0.05$ (12.85%). The proposed adaptive thresholding LASSO control chart also exhibits consistently lower *SDRL* across all shift magnitudes compared to the conventional chart. This indicates that the run length values obtained from the proposed resubmission-based chart have less variability in detecting diagonal/off-diagonal disturbances in the covariance matrix. Specifically, incorporating the resubmission technique into the adaptive thresholding LASSO control chart results in *SDRL* reductions of 11.32%, 21.34%, 31.71%, 22.92%, and 24.90% for shift magnitudes of 0.05, 0.10, 0.15, 0.20, and 0.25, respectively.

Table VI. Run length behavior of competing charts under first diagonal/off-diagonal scenario

Chart	Control limit	Index	δ					
			0	**0.05**	**0.1**	**0.15**	**0.2**	**0.25**
LASSO-RSB	0.2013	*ARL*	204.9480	108.6330	48.8665	22.2605	11.7170	6.5650
		SDRL	210.0123	109.6685	47.7742	21.2081	11.4830	6.0722
		MRL	143.5	70	34	16	8	5
		CT	458.955	88.151	43.010	18.985	10.593	6.539
LASSO-classic	0.2783	*ARL*	200.3697	124.6440	62.9910	31.2335	15.5765	8.7975
		SDRL	200.9690	123.6748	60.7359	31.0542	14.8967	8.0856
		MRL	143.5	82.5	44	22	11	6
		CT	81.960	51.878	25.891	13.981	7.527	4.356

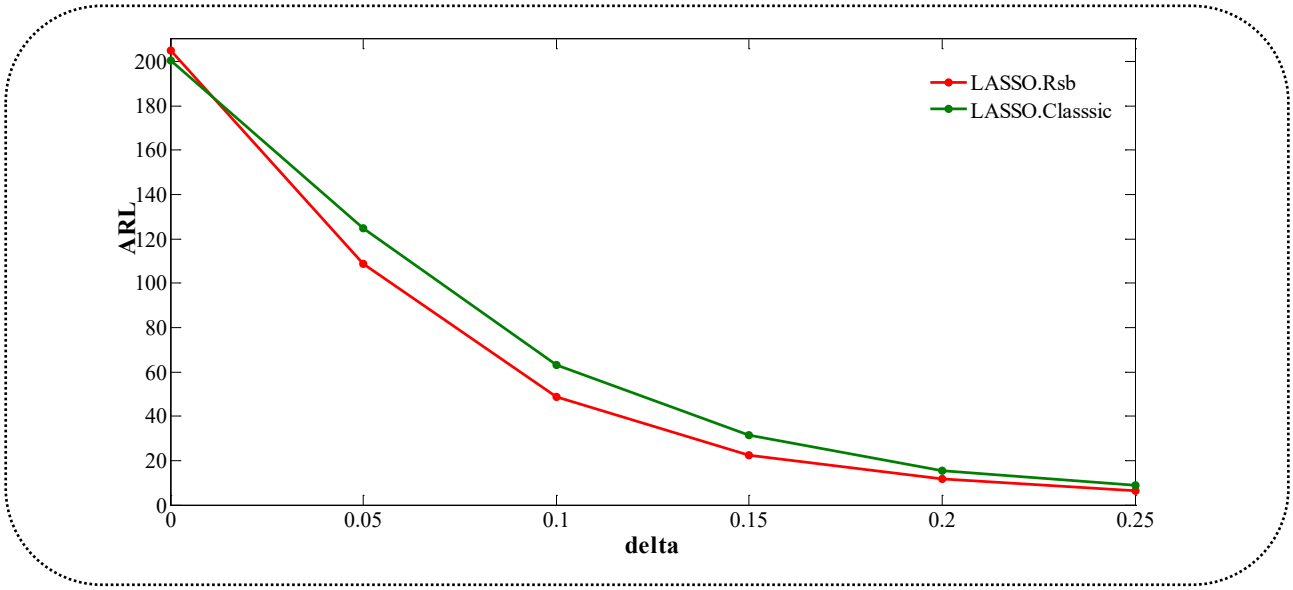

Fig. 6. *ARL* curve for the first diagonal/off-diagonal scenario

Table VII reports the run length characteristics and *CT* values of the classical and resubmission-based versions of the adaptive thresholding LASSO control charts under the second diagonal/off-diagonal shift pattern when $\delta \in \{0.05, 0.1, 0.15, 0.2, 0.25\}$. The findings indicate that, on average, the proposed chart detects a shift of $\delta = 0.05$ approximately 3.66% later than the classical chart. However, for $\delta \geq 0.1$, the proposed chart exhibits a lower *ARL* than

the conventional adaptive thresholding LASSO chart. Additionally, using the resubmission technique in the adaptive thresholding LASSO chart at $\delta \in \{0.1, 0.15, 0.2, 0.25\}$ leads to *ARL* improvements of 5.13%, 6.77%, 7.43%, and 11.49%, respectively. This indicates that the performance enhancement achieved by the proposed chart in terms of the *ARL* index shows an upward trend as the shift magnitude increases.

Table VII. Run length behavior of competing charts under the second diagonal/off-diagonal scenario

Chart	Control limit	Index	δ					
			0	**0.05**	**0.1**	**0.15**	**0.2**	**0.25**
LASSO-RSB	0.2013	*ARL*	204.9480	197.0570	146.2750	108.8975	69.2825	43.3590
		SDRL	210.0123	197.9985	138.8641	105.4267	68.0033	42.4612
		MRL	143.5	136.5	107	75	49	30
		CT	458.955	149.336	125.097	80.579	53.814	33.693
LASSO-classic	0.2783	*ARL*	200.3697	190.1040	154.1895	116.8085	74.8405	48.9880
		SDRL	200.9690	186.4317	149.6332	117.1144	72.0822	49.6714
		MRL	143.5	136	109	83	53	33
		CT	81.960	78.315	66.401	43.020	31.097	20.734

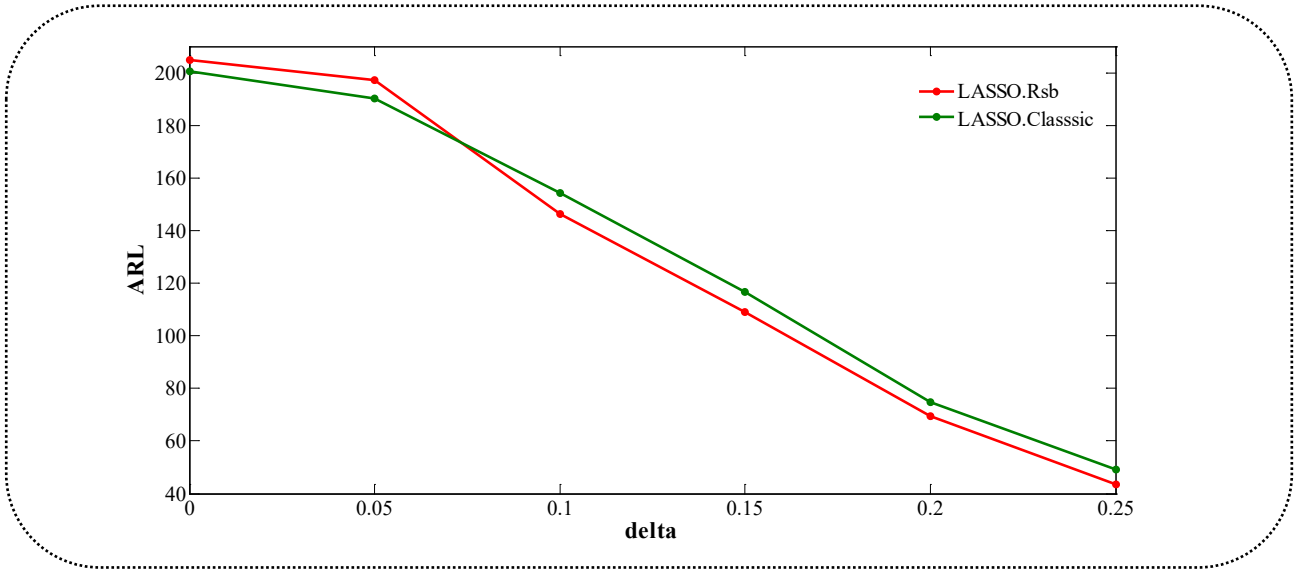

Fig. 7. *ARL* curve for the second diagonal/off-diagonal scenario

Table VIII presents the *ARL*, *SDRL*, *MRL* and *CT* values for the classical adaptive thresholding LASSO control chart and the proposed resubmission-based scheme, evaluated under a third-type joint out-of-control structure, evaluated for shift magnitudes of $\delta \in \{0.05, 0.1, 0.15, 0.2, 0.25\}$. The results indicate that at shift levels of 0.05, 0.10, 0.15, 0.20, and 0.25, the use of the resubmission technique reduces the *ARL* index by 18.7210, 13.9760, 7.6270, 3.4255, and 1.7355 units, respectively. These reductions represent improvements of 18.7%, 30.5%, 35.5%, 32.4%, and 30.3% compared to the classical adaptive thresholding LASSO chart.

Consequently, the proposed resubmission-based adaptive thresholding LASSO chart demonstrates superior

responsiveness in identifying third-type joint diagonal/non-diagonal shifts in the covariance matrix. The most significant improvement, a 35.5% reduction in *ARL*, occurs at $\delta = 0.15$, indicating that the proposed chart is most effective for moderate shift magnitudes.

Table VIII. Run length behavior of competing charts under the third diagonal/off-diagonal scenario

Chart	Control limit	Index	Δ					
			0	**0.05**	**0.1**	**0.15**	**0.2**	**0.25**
LASSO-RSB	0.2013	*ARL*	204.9480	81.4490	31.8275	13.8780	7.1505	3.9845
		SDRL	210.0123	80.7674	31.2204	13.3004	6.8380	3.3641
		MRL	143.5	56	22	10	5	3
		CT	458.955	137.374	58.749	26.990	15.364	10.894
LASSO-classic	0.2783	*ARL*	200.3697	100.1700	45.8035	21.5050	10.5760	5.7200
		SDRL	200.9690	99.8495	45.3963	21.7654	9.8476	5.3838
		MRL	143.5	70	31	15	8	4
		CT	81.960	89.777	46.507	20.304	11.614	8.283

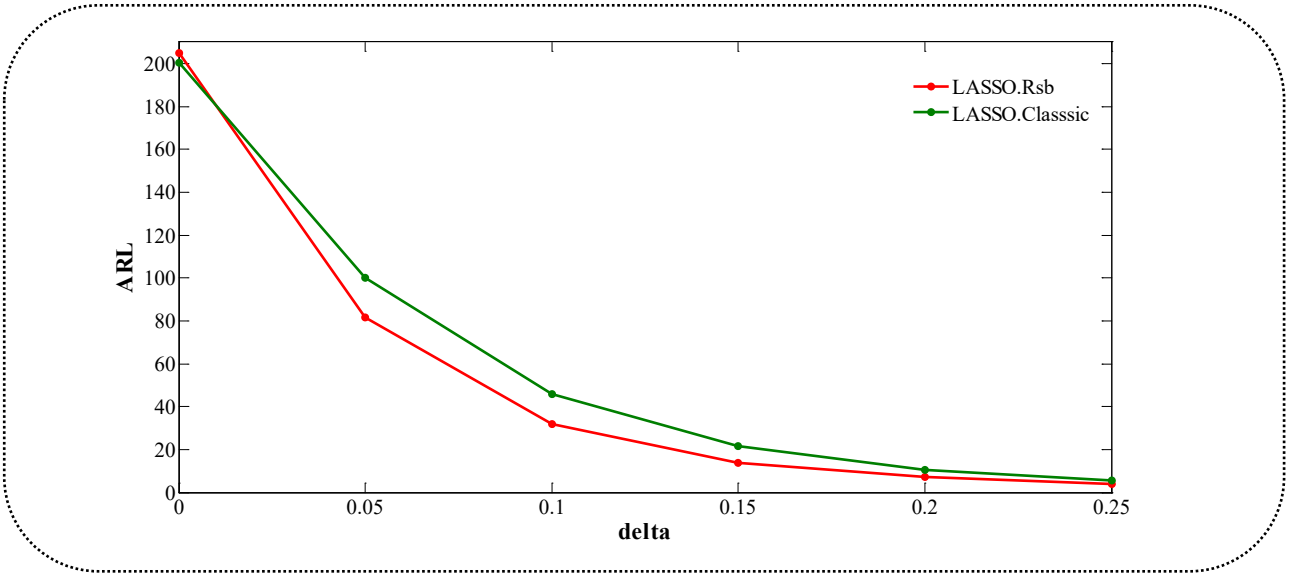

Fig. 8. *ARL* curve for the third diagonal/off-diagonal scenario

V. ILLUSTRATIVE CASE STUDY

This section examines the practical applicability of the proposed LASSO-RSB control chart. It compares this chart with the conventional adaptive thresholding LASSO chart, using a case study from Iran's automotive component industry. Fig. 9 illustrates the component under study, namely the condenser used in the air conditioning system of the Saina automobile, produced by Sardsaz Khodro Company in Golpayegan Industrial Town, Iran. Since the proper operation of the air conditioning system relies on this unit, continuous quality monitoring during its production is essential.

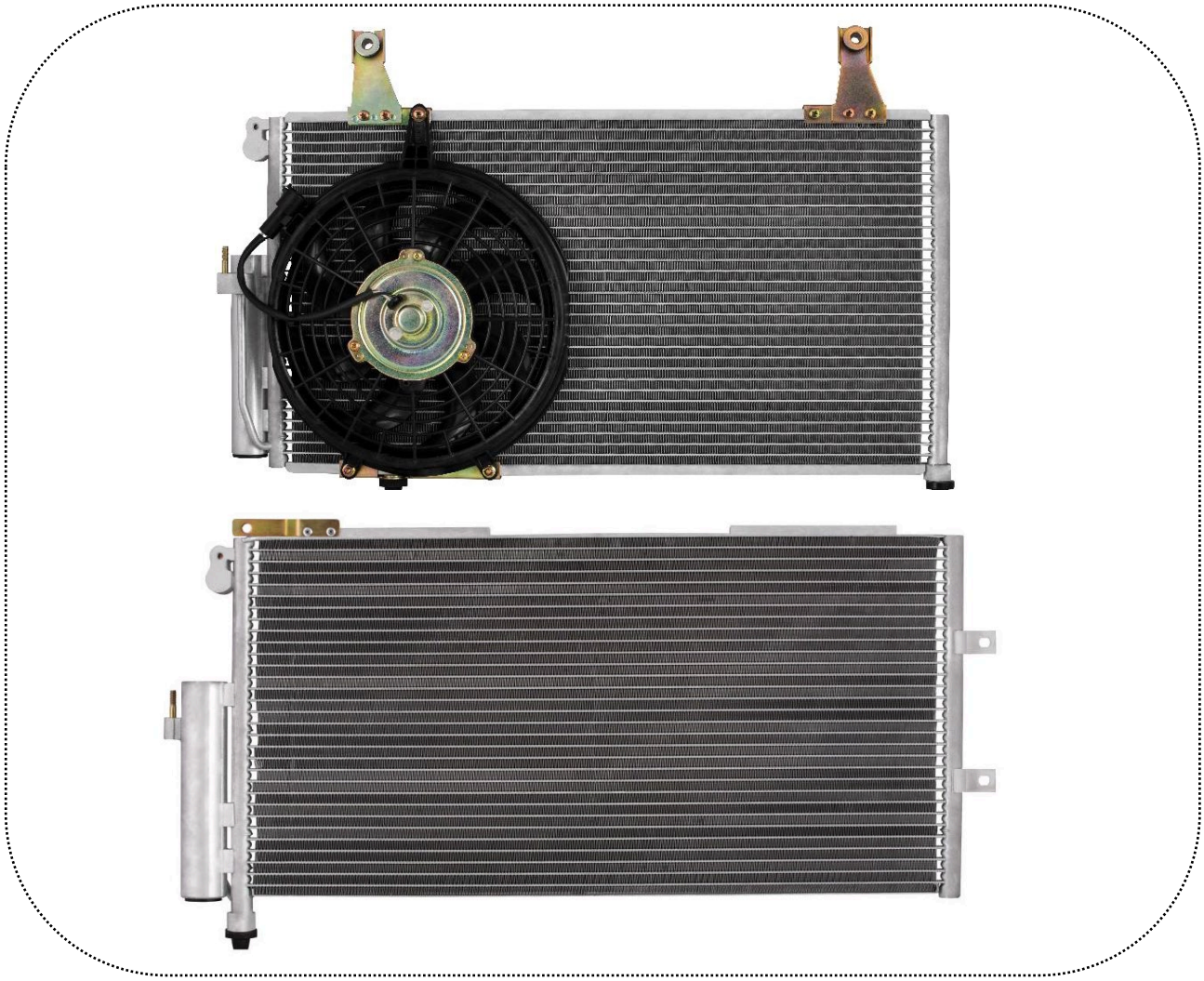

Fig. 9. Condenser component of the Saina automobile air conditioning system

To ensure the quality of manufactured condensers, a precise dimensional inspection process is implemented during production. This process focuses on ten key dimensional characteristics chosen based on the component's geometric properties and structural conditions that may cause distortion or misalignment. The first three quality characteristics (X_1, X_2, X_3) measure the external distances between the right and left collector tubes connected to the condenser core at three positions: upper, middle, and lower. These features assess the dimensional precision and alignment of the condenser core and evaluate any potential distortions that may occur during the furnace brazing process. The inspection process measures the height of individual fins across six specific regions: upper-right, middle-right, lower-right, upper-left, middle-left, and lower-left, for the next six quality features ($X_4, X_5, ..., X_9$). These characteristics assess how the brazing process impacts different types of deformation in the condenser fins. Since the fins are crucial to the condenser's performance, maintaining their dimensional precision is essential for overall system performance. The final quality characteristic (X_{10}) measures the distance between the peak of the flange welded to the left collector tube and the opposing peak of the flange between the two grooves on the same tube. This characteristic assesses how the brazing process impacts flange alignment and the potential distortion of the condenser core during brazing. Any significant deviation in this dimension may indicate misalignment between the flange and the main body of the component. Using $m = 30$ reference samples, each containing $n = 5$ units and $p = 10$ dimensional quality characteristics, we estimate the process mean vector and covariance matrix as follows:

$$\boldsymbol{\mu}_{IC} = \left(632.17, 632.35, 632.17, 7.84, 7.79, 7.75, 7.82, 7.81, 7.79, 39.66\right)^{T} \tag{17}$$

$$\boldsymbol{\Sigma}_{IC} = \begin{pmatrix} +0.5517 & +0.6177 & +0.1782 & +0.0005 & -0.0001 & -0.0231 & -0.0044 & -0.0016 & +0.0028 & +0.1022 \\ +0.6177 & +0.9533 & +0.2822 & -0.0007 & -0.0029 & -0.0331 & -0.0120 & -0.0007 & -0.0049 & +0.0914 \\ +0.1782 & +0.2822 & +0.4079 & +0.0153 & -0.0127 & -0.0151 & -0.0170 & +0.0070 & +0.0018 & +0.0246 \\ +0.0005 & -0.0007 & +0.0153 & +0.0354 & -0.0001 & -0.0090 & +0.0041 & -0.0028 & +0.0010 & +0.0155 \\ -0.0001 & -0.0029 & -0.0127 & -0.0001 & +0.0262 & -0.0030 & +0.0007 & +0.0002 & -0.0009 & +0.0016 \\ -0.0231 & -0.0331 & -0.0151 & -0.0090 & -0.0030 & +0.0395 & -0.0090 & -0.0037 & -0.0012 & -0.0104 \\ -0.0044 & -0.0120 & -0.0170 & +0.0041 & +0.0007 & -0.0090 & +0.0325 & -0.0016 & +0.0020 & +0.0287 \\ -0.0016 & -0.0007 & +0.0070 & -0.0028 & +0.0002 & -0.0037 & -0.0016 & +0.0173 & -0.0004 & +0.0163 \\ +0.0028 & -0.0049 & +0.0018 & +0.0010 & -0.0009 & -0.0012 & +0.0020 & -0.0004 & +0.0235 & +0.0022 \\ +0.1022 & +0.0914 & +0.0246 & +0.0155 & +0.0016 & -0.0104 & +0.0287 & +0.0163 & +0.0022 & +0.5537 \end{pmatrix} \tag{18}$$

Through 50,000 simulation replications, the upper control limit of the proposed LASSO_RSB control charting method is determined to be $UCL'_{A-COV} = 7.7801$, while that of the classical LASSO chart is calculated to be $UCL_{A-COV} = 16.5804$. These control limits ensure a Type I error probability of $\alpha = 0.005$, which is equivalent to $ARL_{IC} = 200$. To demonstrate the implementation of the LASSO-RSB and LASSO-classical charts, we consider out-of-control structure 1, where the variance of each quality characteristic is increased by $\delta = 0.07$ units. The adaptive thresholding LASSO statistics for the generated samples, along with the control limits of both charts, are illustrated in Fig. 10. As shown in Fig. 10, two statistics are presented for samples 4, 14, 21, and 26. To distinguish these samples from the others, the corresponding values are highlighted in red for clarity. For these four samples, the adaptive thresholding LASSO statistic initially exceeds the control limit of the proposed LASSO-RSB chart; however, the statistic obtained in the resubmission falls below the control limit UCL'_{A-COV}, and the process is therefore regarded in-control. In sample 26, the chart statistic obtained in resubmission exceeds the value of $UCL'_{A-COV} = 16.5804$; therefore, the proposed chart issues an out-of-control signal at this point. In contrast, the classical adaptive thresholding LASSO chart indicates that samples 4, 14, 21, and 26 are in-control, while the out-of-control signal is delayed until sample 30. These findings demonstrate that the proposed LASSO-RSB chart can identify the mentioned covariance matrix disturbance four samples earlier than the classical approach, providing superior detection capability.

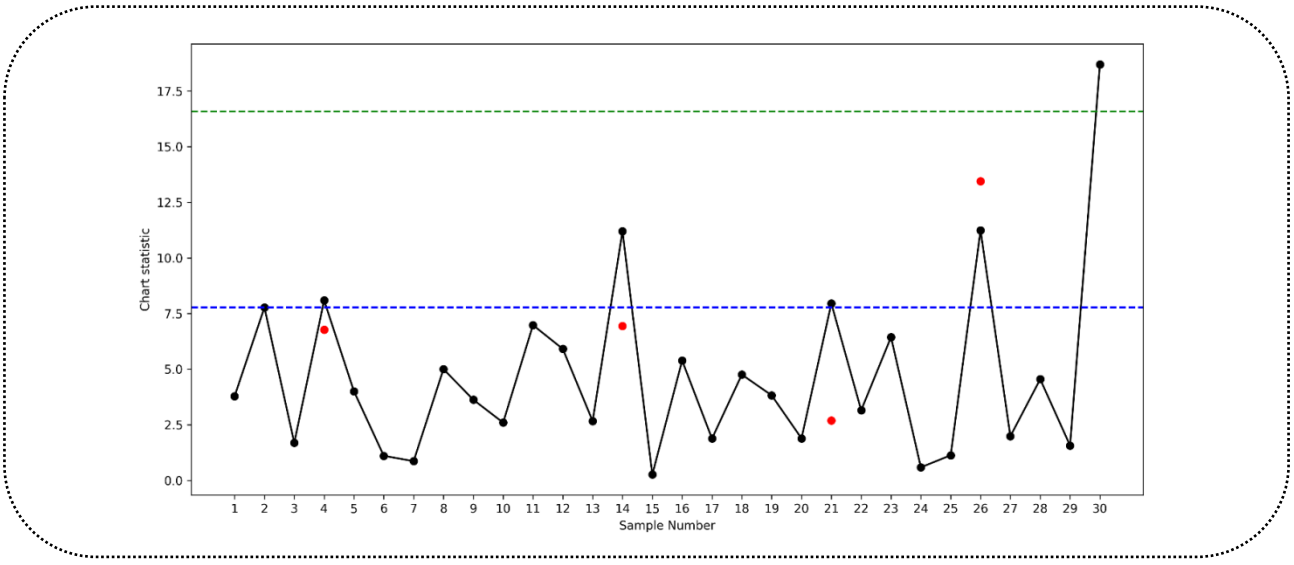

Fig. 10. Adaptive thresholding LASSO statistics with corresponding control limits

VI. CONCLUSION

In many modern industrial and service applications, the greater number of quality characteristics under study than the sample size results in high-dimensional data structures that challenge existing multivariate control charting methods. A significant challenge in monitoring high-dimensional data is the inability of conventional multivariate charts to detect sparse changes in the covariance matrix when only a limited subset of its components is affected by assignable causes. To address this, this study developed an adaptive thresholding LASSO control chart based on the resubmission technique for effective monitoring of the covariance matrix in high-dimensional processes. The performance of the proposed control chart was evaluated against its classical counterpart through Monte Carlo simulations across seven out-of-control scenarios, including diagonal, off-diagonal, and mixed diagonal/off-diagonal covariance matrix structures. The results, analyzed through three key indicators of *ARL*, *SDRL*, and *MRL*, demonstrated that the proposed method consistently outperforms the classical adaptive thresholding LASSO chart in detecting both sparse and non-sparse shifts of small, moderate, and large magnitudes in covariance matrix components. This improvement in the detectability of covariance matrix disturbances, particularly for small to moderate shifts, highlights the capability of the proposed method in high-dimensional monitoring environments such as semiconductor manufacturing, where sensitivity improvement can prevent defective production and yield significant resource savings. This study assumed that successive samples are temporally independent; however, in many industrial and service processes, temporal dependencies among successive observations are inevitable. Extending the resubmission-based adaptive thresholding LASSO chart to account for autocorrelated observations is a promising direction for future research. Furthermore, while this study focuses on statistical performance measures, a cost-benefit analysis of resubmission rounds that balances enhanced chart detectability against increased inspection efforts is essential for future research. Such an extension would provide practical economic guidelines for implementing the proposed chart in industrial environments. Finally, future research could extend the proposed resubmission-based adaptive thresholding LASSO chart to non-normal settings, such as skewed or heavy-tailed distributions, where high-dimensional industrial data may deviate from normality.

FUNDING DECLARATION

The authors declare that no funding was received for the conduct of this research.

REFERENCES

Abdella, G. M., Al-Khalifa, K. N., Kim, S., Jeong, M. K., Elsayed, E. A., & Hamouda, A. M. (2017). Variable selection-based multivariate cumulative sum control chart. *Quality and Reliability Engineering International*, *33*(3), 565-578.

Adeoti, O. A. (2018). A new double exponentially weighted moving average control chart using repetitive sampling. *International Journal of Quality & Reliability Management*, *35*(2), 387-404.

Ahmad, M. R., & Ahmed, S. E. (2021). On the distribution of the T^2 statistic, used in statistical process monitoring, for high-dimensional data. *Statistics & Probability Letters*, *168*, 108919.

Arshad, A., Azam, M., & Aslam, M. (2021). Two successive occasions resubmitted sampling scheme-based control chart. *Quality and Reliability Engineering International*, *37*(3), 950-965.

Arshad, A., Azam, M., Aslam, M., & Jun, C. H. (2024). A resubmission-based variable control chart. *Communications in Statistics-Theory and Methods*, *53*(2), 574-586.

Bodnar, R., Bodnar, T., & Schmid, W. (2024). Control charts for high-dimensional time series with estimated in-control parameters. *Sequential Analysis*, *43*(1), 103-129.

Feng, L., Ren, H., & Zou, C. (2020). A setwise EWMA scheme for monitoring high-dimensional datastreams. *Random Matrices: Theory and Applications*, *9*(02), 2050004.

Govindaraju, K., & Ganesalingam, S. (1997). Sampling inspection for resubmitted lots. *Communications in Statistics-Simulation and Computation*, *26*(3), 1163-1176.

Hajiesmaeili, M., Maleki, M. R., & Salmasnia, A. (2025). Improved adaptive thresholding lasso chart for monitoring dispersion of highdimensional processes using generalized multiple dependent state sampling. *Reliability: Theory & Applications*, *20*(1 (82)), 324-338.

Haq, A. (2024). A new sampling scheme for an improved monitoring of the process mean. *Measurement: Interdisciplinary Research and Perspectives*, *22*(3), 268-279.

Huang, W., Shu, L., Li, Y., & Wang, L. (2023). A phase I change-point method for high-dimensional process with sparse mean shifts. *Naval Research Logistics (NRL)*, *70*(3), 261-273.

Hyder, M., Mahmood, T., Butt, M. M., Raza, S. M. M., & Abbas, N. (2022). On the location-based memory type control charts under modified successive sampling scheme. *Quality and Reliability Engineering International*, *38*(4), 2200-2217.

Jafari, M., Maleki, M. R., & Salmasnia, A. (2023). A high-dimensional control chart for monitoring process variability under gauge imprecision effect. *Production Engineering*, *17*(3), 547-564.

Jalilibal, Z., Karavigh, M. H. A., Maleki, M. R., & Amiri, A. (2024). Control charting methods for monitoring high dimensional data streams: A conceptual classification scheme. *Computers & Industrial Engineering*, *191*, 110141.

Kim, S., & Turkoz, M. (2022). Bayesian sequential update for monitoring and control of high-dimensional processes. *Annals of Operations Research*, *317*(2), 693-715.

Mahmood, T., Hyder, M., & Raza, S. M. M. (2025). Improved EWMA and CUSUM Charts Under Modified Successive Sampling for Monitoring Process Dispersion. *Journal of Statistical Theory and Applications*, 1-33.

Nawaz, T., & Han, D. (2020). Monitoring the process location by using new ranked set sampling-based memory control charts. *Quality Technology & Quantitative Management*, *17*(3), 255-284.

Noor-ul-Amin, M., Tayyab, M., & Hanif, M. (2021). Efficient control charts for monitoring the process mean using different paired double ranked set sampling designs. *Communications in Statistics-Theory and Methods*, *50*(10), 2211-2223.

Oyegoke, O. A., Adekeye, K. S., Olaomi, J. O., & Malela-Majika, J. C. (2025). Hotelling T^2 control chart based on minimum vector variance for monitoring high-dimensional correlated multivariate process. *Quality and Reliability Engineering International*, *41*(2), 765-783.

Rao, G. S., Aslam, M., Alamri, F. S., & Jun, C. H. (2024). Comparing the efficacy of coefficient of variation control charts using generalized multiple dependent state sampling with various run-rule control charts. *Scientific reports*, *14*(1), 2726.

Riaz, M., Mehmood, R., Ali, I., Zaman, B., Khan, N., & Gharib, M. (2025). Generalized multivariate EWMA control chart supplemented with bivariate ranked set techniques. *Quality Technology & Quantitative Management*, *22*(2), 228-256.

Saemian, M., Salmasnia, A., & Maleki, M. R. (2025). A generalized multiple dependent state sampling chart based on ridge penalized likelihood ratio for high-dimensional covariance matrix monitoring. *Scientia Iranica*. In Press, Doi: 10.24200/sci.2022.60169.6640.

Saleh, N. A., Mahmoud, M. A., & Woodall, W. H. (2024). A re-evaluation of repetitive sampling techniques in statistical process monitoring. *Quality Technology & Quantitative Management*, *21*(5), 786-804.

Sun, M., Qian, L., Mukherjee, A., & Xiang, D. (2024). An EWMA chart for high dimensional process with multi-class out-of-control information via random forest learning. *Quality Technology & Quantitative Management*, 1-27.

Ye, H., & Liu, K. (2022). A generic online nonparametric monitoring and sampling strategy for high-dimensional heterogeneous processes. *IEEE Transactions on Automation Science and Engineering*, *19*(3), 1503-1516.

Zhang, S., Xue, L., He, Z., Liu, Y., & Xin, Z. (2023). A sensitized variable selection control chart based on a classification algorithm for monitoring high-dimensional processes. *Quality and Reliability Engineering International*, *39*(7), 2837-2850.

Zhou, W., Wan, Q., Zheng, Y., & Zhou, Y. W. (2017). A joint-adaptive np control chart with multiple dependent state sampling scheme. *Communications in Statistics-Theory and Methods*, *46*(14), 6967-6979.